EPJ Web of Conferences **158**, 02006 (2017) DOI: 10.1051/epjconf/201715802006
QFTHEP 2017

Resonant top pair production at NLO in QCD

Diogo Buarque Franzosi[1,⋆]

[1] *II. Physikalisches Institut, Universität Göttingen, Friedrich-Hund-Platz 1, 37077 Göttingen, Germany*

Abstract.
We compute the contribution of a scalar H or pseudo-scalar A resonance in top-quark pair production at NLO accuracy in QCD including the interference between pure QCD SM diagrams and the resonant $pp \to A(H) \to t\bar{t}$ process which drastically modifies the lineshape of the signal from a simple peak to peak-dip structure. We assume a point-like coupling between scalar and the gluons in a consistent effective field theory framework and improve the results with reweighting techniques in the case of resolved fermion loops in the production. The computation is set in an automatic framework and can be used to produce showered unweighted events. The detailed study is presented in Ref [1].

1 Introduction

Scalar resonances decaying into a $t\bar{t}$ system exist in many BSM scenarios. In order to correctly describe this process at the LHC, and to determine the constraints on the parameters of different models, it is important to get trustworthy and robust theoretical predictions.

It is now known that QCD corrections to this process have a large effect on the total cross section as well as the differential distributions, both for the SM QCD production and for (pseudo-)scalar production. It is also well known that the interference between resonant signal and the QCD background can drastically modify the lineshape of the signal, from a single peak to a dip-peak structure, and may be even larger than the pure signal. It appears to receive similar QCD corrections, as indicated by estimates in an effective field theory (EFT) approach in the soft gluon approximation [2], and in a simplified K-factor derived from the geometric mean of the background and signal K-factors [3].

In this talk, based on Ref [1], we provide the full perturbative calculation of the process $pp(\to A/H) \to t\bar{t}$, at NLO in QCD, including the interference, in the EFT approach, without any further approximation.

Our calculation is performed within the MadGraph5_aMC@NLO (MG5_aMC) [4] framework which allows us to perform automatic simulation of events with parton shower (PS) matching. An interesting feature of our calculation that has not been discussed before is that the gluon-scalar operator mixes into the chromo-magnetic dipole-moment operator, and therefore both operators must be taken into account in a consistent NLO calculation and put together in a coherent setup.

The gluon-gluon-scalar vertex can take two forms depending on the underlying model. If the vertex is dominated by heavy particle loops (e.g. vector-like fermions or scalar top partners), or induced

⋆e-mail: dbuarqu@gwdg.de

by strong dynamics at a high scale, this interaction will not be resolved at the scale of the scalar resonance. In this case the vertex can be simply represented by the dimension-five operators

$$O_{HG} = g_s^2 G^A_{\mu\nu} G^{A\mu\nu} H\,, \tag{1}$$

$$O_{A\tilde{G}} = g_s^2 G^A_{\mu\nu} \widetilde{G}^{A\mu\nu} A\,, \tag{2}$$

with $G^A_{\mu\nu}$ being the gluon field strength tensor and $\widetilde{G}^{A\mu\nu}$ its dual. On the other hand, if the vertex is loop-induced with lighter particles, such as top quarks running in the loop, it will be resolved at the resonance scale and the interaction will give rise to an absorptive phase. It is convenient to distinguish between these two cases, as they often lead to different lineshapes, and the resolved case is more difficult to compute at NLO accuracy. In practice, one may need to deal with a mixed scenario, if there are contributions from both light and heavy loop particles.

Our NLO computation of the interference is based on the EFT framework, which in the unresolved case provides accurate results (i.e. without using soft-gluon approximation), and in the resolved case, can be further improved by using reweighting techniques. These results will then be passed to PS simulation, to obtain more realistic predictions.

2 Theoretical setup

Including only the scalar-gluon operators (Eq. (1)-Eq. (2)) is not enough for a consistent calculation in the EFT. This is because operator mixing with the top-quark dipole moment becomes relevant in this process and including only these operators leads to uncancelled ultra-violet (UV) poles from non-factorisable contributions, whenever a top quark, a gluon and a scalar form a loop, as shown in Figure 1.

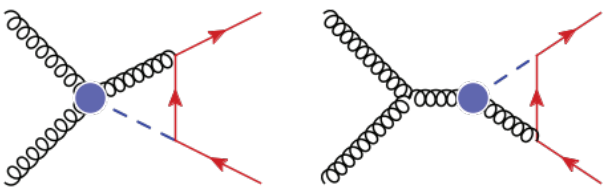

Figure 1. Selected UV divergent diagrams in non-factorisable contributions.

The reason for the UV divergence is not difficult to understand. It is well known that the EFT is renormalisable only if one considers the complete set of higher-dimensional operators up to a certain dimension. However, since so far only the operators O_{HG} and O_{AG} are added, it could mix into a different operator not included in the Lagrangian, leading to non-renormalisability of the theory. In fact, through the triangles shown in Figure 1, the O_{HG} (O_{AG}) induces a chromo-magnetic dipole operator of the top quark, leading to the following self-consistent Lagrangian,

$$L_{Eff} = L_{SM} + y_t \bar{t}tH + \tilde{y}_t \bar{t}i\gamma^5 tA + \frac{C_{HG}}{\Lambda} O_{HG} + \frac{C_{A\tilde{G}}}{\Lambda} O_{A\tilde{G}} + \frac{C_{tG}}{\Lambda} O_{tG}, \tag{3}$$

with the chromo-magnetic dipole operator given by

$$O_{tG} = g_s y_t \bar{t}\sigma^{\mu\nu} T^A t G^A_{\mu\nu}, \tag{4}$$

and O_{HG}, O_{AG} in Eq. (1)-Eq. (2). We include also Yukawa couplings between H, A and top quark.

If the full theory is known, one can determine the Wilson coefficient by explicitly computing the vertex in the full theory. For example, if this contribution is induced by a vector-like fermion, F, via the following Yukawa interactions:

$$L_{Yuk} = y_F \bar{F} F H + \tilde{y}_F F i\gamma^5 F A \,, \tag{5}$$

the matching of O_{HG} and O_{AG} coefficients can be performed in the usual way by identifying the triagle diagram with the vertex at LO and with an extra loop at NLO, and the O_{tG} can be matched with the two-loop Barr-Zee diagram [5], resulting in the following identification

$$\frac{C_{HG}(m_F)}{\Lambda} = -\frac{y_F}{48\pi^2 m_F} - \frac{11\alpha_s y_F}{192\pi^3 m_F} + O(\alpha_s^2)\,, \tag{6}$$

$$\frac{C_{A\tilde{G}}(m_F)}{\Lambda} = -\frac{\tilde{y}_F}{32\pi^2 m_F} + O(\alpha_s^2)\,, \tag{7}$$

$$\frac{C_{tG}(m_F)}{\Lambda} = -\frac{\alpha_s}{1152\pi^3 m_F}\left(8y_F - 9\tilde{y}_F\frac{\tilde{y}_t}{y_t}\right) + O(\alpha_s^2). \tag{8}$$

The matching procedure is obviously dependent on the specific underlying model.

On the other hand, the running and mixing of the effective coefficients are model-independent. We perform the calculation at the renormalisation scale μ, conventionally chosen at $\mu = m_H/2$ ($m_A/2$). In case the scale m_F and μ are well separated, one needs to run the EFT from m_F down to μ to resum the large logarithmic contributions. For $O(\alpha_s)$ mixing this is done by solving the RG equations

$$\frac{dC_i(\mu)}{d\log\mu} = \frac{\alpha_s(\mu)}{\pi}\gamma_{ij}C_j(\mu)\,, \tag{9}$$

where for the three operator coefficients $C_{HG}, C_{A\tilde{G}}, C_{tG}$, the matrix γ_{ij} is given by

$$\gamma = \begin{pmatrix} 0 & 0 & 0 \\ 0 & 0 & 0 \\ -1 & \tilde{y}_t/y_t & 1/3 \end{pmatrix}. \tag{10}$$

The coefficients at a given scale μ are thus given by

$$C_i(\mu) = \exp\left(\frac{-2}{\beta_0}\log\frac{\alpha_s(\mu)}{\alpha_s(m_F)}\gamma_{ij}\right)C_j(m_F)\,, \tag{11}$$

where $\beta_0 = 11 - 2/3 n_f$, and $n_f = 5$ is the number of running flavors.

The above procedures take into account the $O(\alpha_s)$ mixing from $O_{HG,A\tilde{G}}$ to O_{tG}. The mixing from O_{tG} to O_{HG} also exists, but is of order $O(y_t^2)$, and is negligible because $|C_{tG}| \ll |C_{HG}|$ (C_{tG} is two-loop induced).

Once $C_i(\mu)$ is known, NLO predictions based on the EFT can be computed. In this work we use the automated framework based on MG5_aMC. Calculations at NLO with higher-dimensional operators have been recently performed for the top-quark sector of the SMEFT [6–10].

The approach described above provides the exact NLO QCD prediction for the EFT, which is a good approximation if the ggH (ggA) vertex is induced by heavy particles with masses larger than $m_{H(A)}/2$. For lighter particles, in particular the top quark which always couples directly to the scalar, the EFT is not valid anymore, since it fails to capture the absorptive part of the loop, which is crucial for describing the lineshape. To partially improve this situation we perform an event-by-event reweighting [11] procedure using the ratio of Born amplitudes $|M_{\text{exact}}|^2/|M_{\text{EFT}}|^2$ as ratio, with complex effective coefficients to avoid divergent ratios for the interference.

3 Benchmarks and results

To study the lineshape, we will perform the calculation for several benchmark models, which cover both the resolved and unresolved cases. The impact of QCD corrections in our EFT approach will be illustrated by the first two benchmark models, where the $ggH(A)$ vertex is not resolved. In the first scenario, we consider a CP-even scalar that couples to a heavy vector-like fermion doublet, which induces the ggH vertex at one loop. The matching procedure discussed in the previous section can be explicitly carried out. In the second model, we consider a CP-odd scalar as a pseudo-Goldstone boson of new strong dynamics, whose decay into top-quarks may shed light on an eventual dynamical fermions mass generation [12, 13].

For our final benchmark scenarios we consider the CP-even and CP-odd Higgses of the 2HDM. In this case the top-loop induced $ggH(A)$ vertex is fully resolved as only top and bottom quarks run in the loops. For these benchmarks we construct the EFT and improve our predictions by Born-reweighting.

For the results shown here we fix our EFT scale at one half of the scalar resonance mass, while for renormalisation and factorisation scales we choose a dynamical scale equal to one half of the sum of the transverse masses in the final state. We vary the scales independently by a factor of two up and down to estimate the scale uncertainties. The Yukawa coupling between the H and the top quark is renormalised by $\overline{MS}$ scheme but fixed at the scale $m_H/2$. We use the LO and NLO NNPDF2.3 parton distribution functions [14] for the corresponding computation. We obtain results both at fixed-order and also matched to the parton shower with MC@NLO [15]. For parton shower we always use Pythia8 [16].

3.1 Benchmark A

Consider a vector-like quark doublet, F, with Yukawa coupling to a CP-even scalar H described by Eq. (5). We choose the following parameters:

$$m_H = 500\ \text{GeV},\ \Gamma_H = 40\ \text{GeV},\ m_F = 500\ \text{GeV}, \tag{12}$$

$$y_t = 0.4,\ y_F = 5. \tag{13}$$

The ggH vertex from the F fermion running in the loop is given by Eq. **??**, multiplied by a factor of two. For the top-quark loop, we simply replace m_F by m_t and y_F by $y_t/\sqrt{2}$. This does not fully capture the top-loop contribution, in particular the phase, however given that the dominant contribution is coming from the F fermion, the EFT is still a very good approximation.

Using Eqs. (6), (8), and (11), we find the following operator coefficients, at scale $\mu_{EFT} = m_H/2$:

$$\frac{C_{HG}}{\Lambda} = -5.11 \times 10^{-5}\ \text{GeV}^{-1}, \tag{14}$$

$$\frac{C_{tG}}{\Lambda} = -1.40 \times 10^{-6}\ \text{GeV}^{-1}, \tag{15}$$

where we have taken m_t to be 172.5 GeV. The above values define our EFT.

In the left panel of Figure 2 we show the fixed order $m_{t\bar{t}}$ distribution. Signal and interference lineshapes are displayed separately. The signal peaks at the resonant mass 500 GeV, and the radiative correction is quite large as expected. In particular, we observe an increasing K-factor as the $t\bar{t}$ invariant mass moves away from the resonance to lower values. On the right panel, the same results are shown but matched to the PS. Compared with the fixed order result, the size of the radiative corrections is now tamed below the resonance, mainly because the emission from decay products is partly taken into account by the PS. The K-factor for the signal is in general flat, with a small enhancement near

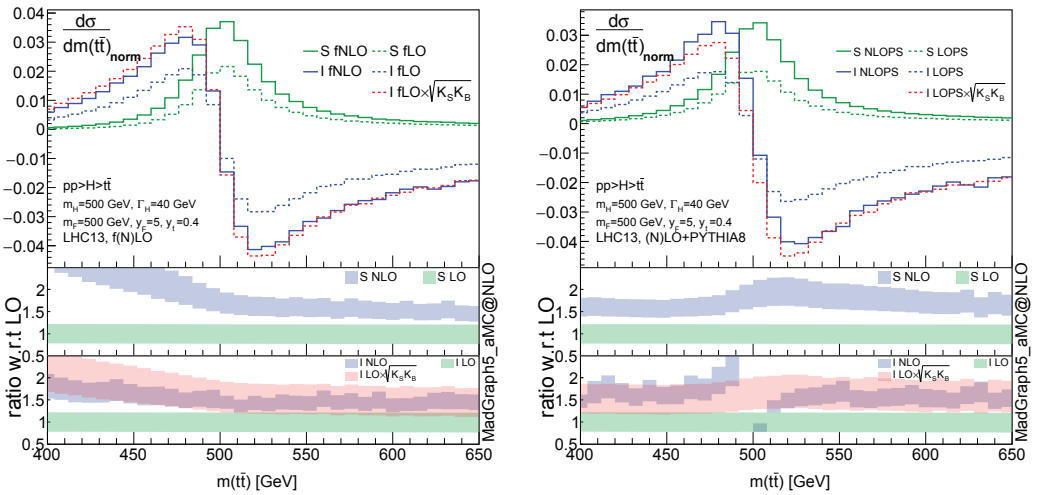

Figure 2. Signal and interference lineshapes at at (N)LO fixed order (*left*) and matched with PS (*right*) for LHC 13 TeV. Results are normalised to the SM fNLO lineshape. Lower panels show the K-factors and the scale uncertainties of signal and interference respectively.

the peak. In contrast, the K-factor for the interference shows a peak-dip structure, mainly because the zero point has been slightly shifted. This effect is not reproduced by a K-factor rescaling used in Ref. [3]. As one can see in the last panel, the inferred K-factor $\sqrt{K_S K_B}$ is flat and does not reproduce the peak-dip structure, and as a result this approximation will predict an interference lineshape that is shifted to the left compared with our full calculation. Finally, compared with the fixed-order results, the showered lineshape has a slightly lower peak due to smearing effects.

3.2 Benchmark B

As a benchmark of CP-odd state we consider the models of partial compositeness of Ref. [13], more specifically the a state of M3 model with $(n_\psi, n_\chi) = (-4, 2)$ in the η' decoupling limit, $\alpha = \zeta$. We choose the compositeness scale $f = 800$ GeV and the mass $m_a = 1$ TeV. The relevant couplings of $A \equiv a$ in Eq. (3) are [1]:

$$\frac{C_{A\tilde{G}}}{\Lambda} = -2.15308 \times 10^{-5}\ \text{GeV}^{-1}\,, \tag{16}$$

$$\tilde{y}_t = -0.571406\,. \tag{17}$$

The $O_{A\tilde{G}}$ operator is generated through the axial-vector anomaly which couples the technipions to a pair of gauge bosons. We assume

$$C_{tG}(1\ \text{TeV}) = 0\,. \tag{18}$$

The total width is dominated by the top decay and has some correction from di-gluon decay and is given by

$$\Gamma_A = 37.5\ \text{GeV}\,. \tag{19}$$

[1]The conversion from parameters defined in Ref. [13] to our convention in Eq. (3) is given by: $\frac{C_{A\tilde{G}}}{\Lambda} = \frac{\kappa_g}{16\pi^2 f_\pi^2}$ and $\tilde{y}_t = C_t \frac{m_t}{f_\pi}$.

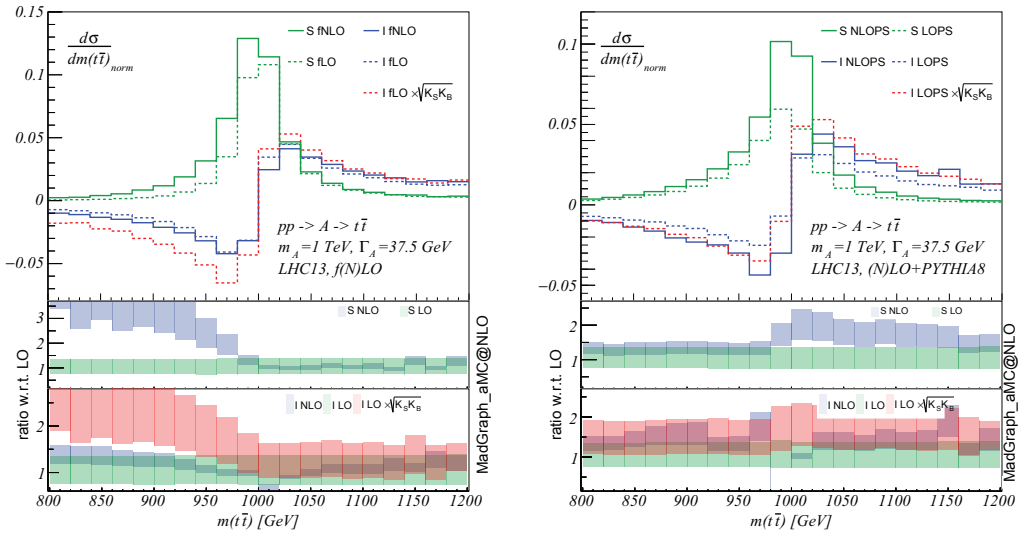

Figure 3. Signal and interference lineshapes at (N)LO fixed order (*left*) and matched with PS (*right*) for LHC 13 TeV. Results are normalised to the SM fNLO lineshape. Lower panels show the K-factors and the scale uncertainties of signal and interference respectively.

It is interesting to note that $C_{A\tilde{G}}$ and $\tilde{y}_t$ have the same sign and this implies that the top coupling has an opposite contribution to the gluon coupling, creating a dip-peak structure instead of the usual peak and dip. This opposite contribution also generates some strong cancellations if one approximates the full top loop with a heavy fermion, as we have done for benchmark A, thus for this benchmark we use only the effective coefficient generated by the high scale physics and neglect the top loop in the gluon coupling.

In Figure 3 we show the invariant mass distribution of the top pair system $m_{t\bar{t}}$ at fixed order in perturbation theory in the left and the result matched with PS in the right. In the upper panel the NLO and LO predictions are shown normalised bin-by-bin to the background QCD prediction.

3.3 Benchmarks C1 and C2

For our final BSM scenario we employ the 2HDM [17], which introduces a second $SU(2)_L$ doublet Φ_2 and gives rise to five physical Higgs bosons: one light (heavy) neutral, CP-even state h (H); one neutral, CP-odd state A; and two charged Higgs bosons $H^{\pm}$. In this work we take h to be the 125 GeV Higgs. The input parameters determining all properties of a 2HDM scenario are:$\tan\beta$, $\sin\alpha$, m_h , m_H , m_A , $m_{H^{\pm}}$, m^2_{12} with the convention $0 \leq \beta - \alpha < \pi$ (with $0 < \beta < \pi/2$).

The ratio of the Yukawa couplings over the SM values are $\sin\alpha/\sin\beta$ and $\cot\beta$ for H and A respectively. We chose two benchmark scenarios whose parameters are listed in Table (1). Electroweak precision tests, the LHC Higgs results and searches for heavy scalar particles, along with unitarity, perturbativity and vacuum stability constrain the parameter space of the model. In the selection of 2HDM benchmarks, these constraints are taken into account.

	Type	$\tan\beta$	$\sin(\beta-\alpha)$	m_H	m_A	$m_{H^\pm}$	m_{12}^2
C1	I	2.0	1.0	300	450	450	20000
C2	II	0.9	1.0	450	600	620	10000

Table 1. Parameter choices for the 2HDM benchmarks used in our study. All masses are given in GeV. The light Higgs mass is fixed to $m_h = 125$ GeV.

In benchmark C1 only the pseudoscalar Higgs lies above the top–anti-top threshold. The corresponding Yukawa couplings (as rescalings of the SM Higgs top Yukawa) are: $g_t^H = -0.5$ and $g_t^A = 0.5$. The heavy scalar width is negligible while the pseudoscalar width is $\Gamma_A = 7.35$ GeV and the top quark decay branching fraction is approximately 65%.

Following Eqs. (6), (8), and (11), we find the following operator coefficients, at scale $\mu_{EFT} = m_A/2$:

$$\frac{C_{HG}}{\Lambda} = 4.73 \times 10^{-6}\ \text{GeV}^{-1}\,, \tag{20}$$

$$\frac{C_{AG}}{\Lambda} = -6.49 \times 10^{-6}\ \text{GeV}^{-1}\,, \tag{21}$$

$$\frac{C_{tG}}{\Lambda} = 9.56 \times 10^{-9}\ \text{GeV}^{-1}\,. \tag{22}$$

Where we have taken m_t to be 172.5 GeV.

The corresponding couplings and widths for benchmark C2 are: $g_t^H = -1.11$, $g_t^A = 1.11$, $\Gamma_H = 10.7$ GeV and $\Gamma_A = 38.7$ GeV. Both resonances decaying almost exclusively to top quarks with the relevant branching fractions being $Br(H \to t\bar{t}) = 0.995$ and $Br(A \to t\bar{t}) = 0.921$.

The operator coefficients at scale $\mu_{EFT} = m_A/2$ are:

$$\frac{C_{HG}}{\Lambda} = 1.05 \times 10^{-5}\ \text{GeV}^{-1}\,, \tag{23}$$

$$\frac{C_{AG}}{\Lambda} = -1.44 \times 10^{-5}\ \text{GeV}^{-1}\,, \tag{24}$$

$$\frac{C_{tG}}{\Lambda} = 4.11 \times 10^{-8}\ \text{GeV}^{-1}\,. \tag{25}$$

The above values define our EFT. For these scenarios, the EFT is not expected to accurately describe the lineshape as the top-loop is resolved. In order to improve the result we reweight event-by-event with the full one-loop LO amplitude $|M_{\text{exact}}|^2/|M_{\text{EFT}}|^2$. To carry out this procedure we must avoid division by zero and for that we incorporate a phase to the coefficients $\frac{C_{AG}}{\Lambda} \to (a + bi) \times \frac{C_{AG}}{\Lambda}$, where a and b are extracted by matching the exact and EFT amplitudes at leading order in particular at the point where they cross zero.

Differential results for the 2HDM benchmarks C1 and C2 are shown in Figure 4 left and right respectively. The invariant mass distribution of the top quark pair is computed at (N)LO+PS, with the signal and interference contributions and their corresponding K-factors displayed separately. The LO results are exact, i.e. they include the full top mass dependence, while for the NLO results we use the phase-improved EFT to compute the NLO corrections and then apply a Born-reweighting at an event-by-event level. As the reweighting is based on event generation we present only (N)LO+PS for these benchmarks. Results obtained using the approximate average K-factor, $\sqrt{K_S K_B}$, are also shown. For both benchmarks the signal K-factors peak around the resonant masses. The interference

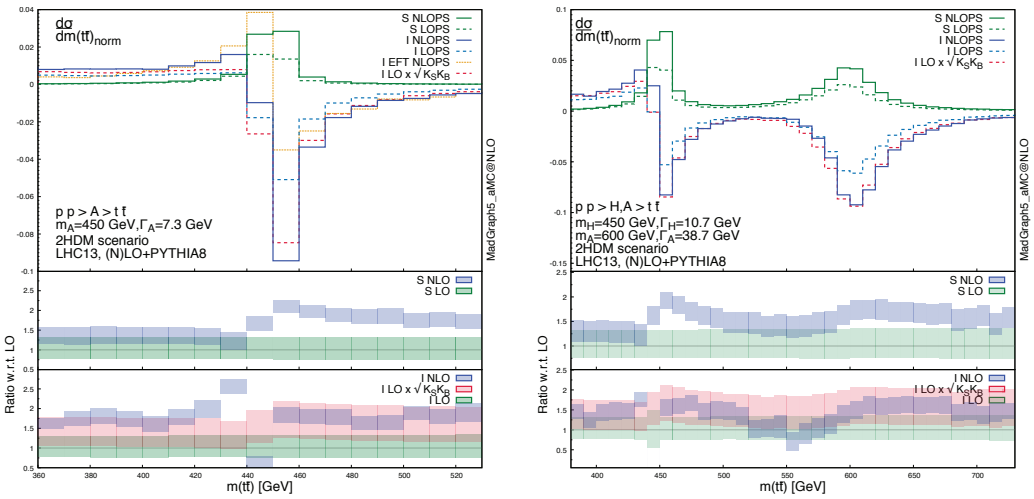

Figure 4. Signal and interference lineshapes at (N)LO matched with PS for LHC 13 TeV. Results are normalised to the SM fNLO lineshape. Lower panels show the K-factors and the scale uncertainties of signal and interference respectively.

$K-$factor shows a peak-dip structure as the NLO corrections shift the zero crossing point from its LO position. The approximate K-factor, $\sqrt{K_S K_B}$ is much flatter, with small peaks driven by the peaks in the signal K-factor at the resonance masses. Moreover, the uncertainties of that prediction are much larger as they are by construction LO.

For benchmark C1 we also show in yellow the prediction obtained for the interference in the EFT limit, i.e. without any reweighting. As expected the EFT prediction does not a provide a good description of the interference lineshape.

We stress that for scenarios where two resonances are present the experimental resolution will be crucial to establish whether one or two peaks are visible in the invariant mass distribution. For our benchmark the mass difference of 150 GeV should be sufficiently large. We note that here the interference distribution suffers from low statistics in the region between the two resonance masses, where the cross-section is very small.

4 Conclusions

The NLO QCD corrections to the interference between signal and background in resonant scalar or pseudoscalar top pair production have been computed using an EFT approach without any approximations. In this way we obtained accurate predictions for the $t\bar{t}$ lineshape for the case in which gluon fusion scalar production is dominated by heavy particles running in the loop or strong dynamics generating point-like interaction between the scalars and the gluon. The QCD corrections are important and cannot be correctly described by approximations.

A non-trivial feature of the calculation is the mixing between the gluon-scalar operators and the chromo-magnetic dipole operator, which implies that both operators and their mixings must be incorporated in the computation in order to extract meaningful physical results.

In addition, to treat the cases where loops of “light" fermions, like the top-quark itself, dominate the gluon fusion scalar production and thus the EFT approach is not immediately applicable, we have shown that our calculation can still be used. For that we introduced a phase to the Wilson coefficients to reproduce the absorptive part of the one-loop amplitude, and by reweighting the amplitudes using the exact LO amplitudes we obtained results beyond LO.

Our calculation is fully automated and can be matched to PS programs through the MG5_aMC program. We have presented results for a set of benchmark scenarios including pseudo-scalars and scalars in resolved and unresolved cases. We found that QCD corrections are important, increasing the yields and modifying the distribution with non-trivial K-factors, as well as reducing the scale uncertainties of the predictions.

We expect our predictions, combined with advances in experimental strategies, will improve the sensitivity in searches for BSM scalars in $t\bar{t}$, by reducing the systematical uncertainty from the theory side, and by optimising the experimental strategies according to an accurate lineshape description. Moreover, they will also allow the extraction of more reliable constraints on the parameters of various BSM models.

The reader is encouraged to read our full work in Ref. [1], where we give more details on the calculation and more extensive discussion, for instance about the impact of the uncertainty due to the treatment of the interference contribution in the matching to PS simulation and matching between underlying theory and EFT parameters.

References

[1] D. Buarque Franzosi, E. Vryonidou, C. Zhang (2017), 1707.06760
[2] W. Bernreuther, P. Galler, C. Mellein, Z.G. Si, P. Uwer, Phys. Rev. **D93**, 034032 (2016), 1511.05584
[3] B. Hespel, F. Maltoni, E. Vryonidou, JHEP **10**, 016 (2016), 1606.04149
[4] J. Alwall, R. Frederix, S. Frixione, V. Hirschi, F. Maltoni et al., JHEP **1407**, 079 (2014), 1405.0301
[5] S.M. Barr, A. Zee, Phys. Rev. Lett. **65**, 21 (1990), [Erratum: Phys. Rev. Lett.65,2920(1990)]
[6] C. Degrande, F. Maltoni, J. Wang, C. Zhang (2014), 1412.5594
[7] D. Buarque Franzosi, C. Zhang, Phys. Rev. **D91**, 114010 (2015), 1503.08841
[8] C. Zhang, Phys. Rev. Lett. **116**, 162002 (2016), 1601.06163
[9] O. Bessidskaia Bylund, F. Maltoni, I. Tsinikos, E. Vryonidou, C. Zhang, JHEP **05**, 052 (2016), 1601.08193
[10] F. Maltoni, E. Vryonidou, C. Zhang, JHEP **10**, 123 (2016), 1607.05330
[11] O. Mattelaer, Eur. Phys. J. **C76**, 674 (2016), 1607.00763
[12] T. Alanne, M.T. Frandsen, D. Buarque Franzosi, Phys. Rev. **D94**, 071703 (2016), 1607.01440
[13] A. Belyaev, G. Cacciapaglia, H. Cai, G. Ferretti, T. Flacke, A. Parolini, H. Serodio, JHEP **01**, 094 (2017), 1610.06591
[14] R.D. Ball, V. Bertone, S. Carrazza, L. Del Debbio, S. Forte, A. Guffanti, N.P. Hartland, J. Rojo (NNPDF), Nucl. Phys. **B877**, 290 (2013), 1308.0598
[15] S. Frixione, B.R. Webber, JHEP **06**, 029 (2002), hep-ph/0204244
[16] T. Sjostrand, S. Mrenna, P.Z. Skands, Comput. Phys. Commun. **178**, 852 (2008), 0710.3820
[17] G. Branco, P. Ferreira, L. Lavoura, M. Rebelo, M. Sher et al., Phys.Rept. **516**, 1 (2012), 1106.0034